42

Turbulence and mixing regimes specific to lakes

ANDREAS LORKE
(andreas.lorke@uni-konstan.de)
and ALFRED WÜEST

42.1 Introduction

This chapter considers phenomena of turbulent mixing that are specific and special to lakes. Most stratified turbulence processes, as depicted in Fig. 42.1 for lakes, occur both in the oceans and in lakes, and most of them are described in detail elsewhere within this book. The similarities to oceanic methods, observations, and theories are manifold. Comprehensive overviews of the hydrodynamics of lakes in a more general sense are given, for instance, by Mortimer (1974), Hutter (1983), Imberger and Patterson (1990), Imboden and Wüest (1995), and Imberger (1998). Therefore, we will focus (a) specifically on turbulence and (b) on phenomena that are (i) either more important or (ii) more easily observed in lakes.

The methods and measurement techniques for the observation of turbulence and the estimation of turbulent mixing in lakes have been developed in parallel or subsequent to their oceanographic counterparts described in Part II of this book (for a historical review see also Gregg (1991)). For many studies, the method of choice was the temperature microstructure method described briefly in Section 12.4.2 of this book (see also the major contributions to this important method by Dillon and Pearson (1981), Imberger (1985), Brubaker (1987), Imberger and Ivey (1991), MacIntyre (1993), Crawford and Collier (1997), and Luketina and Imberger (2001)). The main advantage of this method is the low detection limit, which is capable of resolving the rather weak turbulence within the stratified waters of lakes. Recent technological developments are able to resolve the turbulent current fluctuations using laser Doppler anemometry (Etemad-Shahidi and Imberger, 2001) or coherent acoustic Doppler methods (Lhermitte and Lemmin, 1990; Lohrmann *et al.*, 1990). The latter are discussed as CDVPs in greater detail in Chapter 15 of this volume.

According to the dominant physical forcing mechanisms, the lake's water body can be divided into three different compartments: the (intermittently stratified) surface boundary layer (SBL), the bottom boundary layer (BBL), and the stratified interior in between. We notice that this physically oriented subdivision is not fully identical with the common limnologic subdivision of lakes into epilimnion, metalimnion, and hypolimnion.

The goal of this chapter is to summarize the typical turbulence characteristics within the above three physical compartments as observed by efforts within the last two decades, and to conclude with a synthesis, describing the flux path of mechanical energy within and between these compartments.

42.2 The surface boundary layer

The SBL is the interface between the stratified bulk of the lake and the atmosphere. Wind stress and/or surface buoyancy flux usually supply the energy required to establish a surface mixed layer. However in the case of a negative surface buoyancy flux (heating of the lake surface) and perfectly calm conditions, thermal stratification can reach the surface and reflect the absorption of short-wave radiation (e.g. Fig. 42.6(a)) later. The uppermost part of the water column, in which mixing and stratification directly follow the diurnal cycle of atmospheric forcing, is called the diurnal mixed layer (Imberger, 1985). The various forcing mechanisms produce different patterns of turbulent mixing within this layer, which can be described using various scaling laws. In the following sections we will focus on (perfectly separated) forcing conditions of wind-driven turbulence and convective mixing as they were studied in numerous lakes.

42.2.1 Wind-driven turbulence

Wind introduces turbulence kinetic energy (TKE) into the lake by creating a stress τ_0 on the lake surface. This stress is related to the wind speed W_{10} via the drag coefficient C_{10}:

$$\tau_0 = \rho_{\mathrm{air}} C_{10} W_{10}^2, \tag{42.1}$$

where $\rho_{\mathrm{air}} = 1.25\ \mathrm{kg/m^{-3}}$ is the density of air and the subscript 10 refers to the height in meters above the lake surface at which the wind speed was measured. Assuming a constant stress layer across the air/water interface and within the upper water column, it can be shown using dimensional arguments that the functional dependence of the horizontal velocity within the water u is given by the law of the wall (LOW),

$$\frac{\partial u}{\partial z} = -\frac{u_{\mathrm{f}}}{\kappa z}, \tag{42.2}$$

Marine Turbulence: Theories, Observations, and Models. Results of the CARTUM Project, ed. Helmut Z. Baumert, John Simpson, and Jürgen Sündermann. Published by Cambridge University Press.

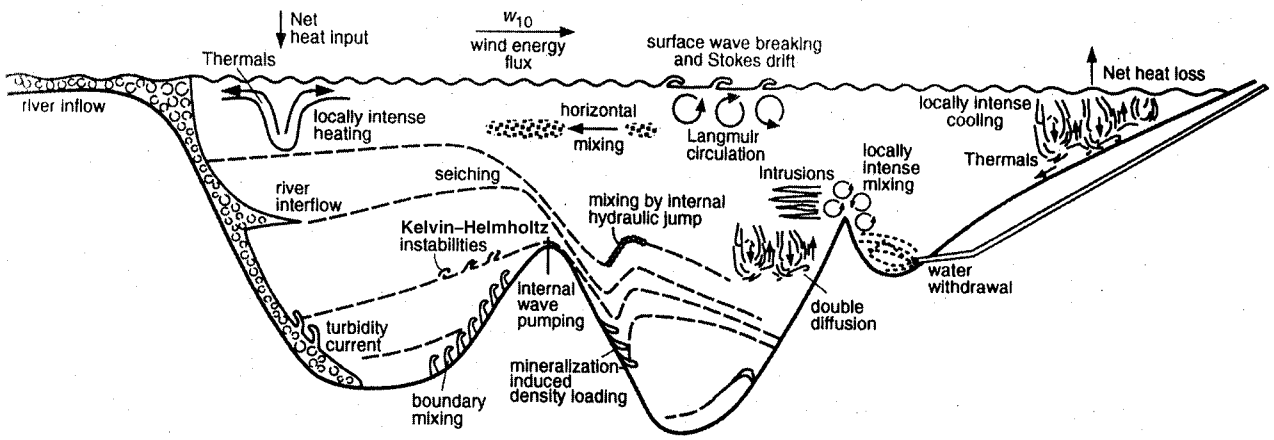

Fig. 42.1. A schematic overview of mixing processes in lakes. From Imboden and Wüest (1995). Copyright 1995 Springer-Verlag.

where $\kappa = 0.41$ is the von Kármán constant, ρ is the density of the water, z is the depth, measured positive downward, and u_f is the so-called friction velocity calculated from the surface shear stress τ_0 via $u_f^2 = \tau_0/\rho$. Integration of the above equation yields the well-known logarithmic velocity profile. Assuming, furthermore, homogeneous and stationary conditions (production of TKE equals dissipation), the dissipation rate ε within the non-stratified water column should scale with the cube of the wind speed W_{10} and decrease reciprocally with depth:

$$\varepsilon(z) = \left(\frac{\rho_{\text{air}} C_{10}}{\rho}\right)^{3/2} \frac{{W_{10}}^3}{\kappa z}. \tag{42.3}$$

Measured profiles of dissipation rates, as shown in Fig. 42.2(a), fit quite well to the reciprocal-depth dependence of the scaling relation (42.3) – an observation already made by Dillon and Pearson (1981). Although the observed functional form of $\varepsilon(z)$ is in good agreement with (42.3), the absolute scaling of TKE dissipation remains difficult due to (1) the kinematics of the surface waves and (2) the non-constancy of the drag coefficient C_{10}.

Results of a recent study by A. Simon, O. Kocsis, and A. Wüest (not yet published) in Lake Neuchâtel (Switzerland) showed that the observed wind produced on average about half of the TKE found for the same wind speed under equivalent oceanic conditions (Fig. 42.2(c). The reason for this observation is that the atmospheric stress (τ_0) is split up at the air/water interface into stress accelerating the waves (τ_w) and stress accelerating the water (τ_{LOW}); i.e. $\tau_0 = \tau_w + \tau_{\text{LOW}}$. As a result, $u_f = \sqrt{\tau_0/\rho}$ inferred from atmospheric stress is an overestimate for the turbulence level in the LOW layer, which is characterized by τ_{LOW}/ρ only, and consequently $\varepsilon(z)$ according to (42.3) would result in an overestimate of the turbulence dissipation.

They found that, at low wind speeds, the drag coefficient C_{10} is not constant but consistently increases with decreasing winds, approximately inversely proportionally to the speed (Fig. 42.2(c)) – an effect that can be attributed to "laminarization" at very low levels of turbulence (Wu, 1994). Whereas roughness is determined by the increasing wave height for strong winds, it has, surprisingly, been realized that roughness is obviously greater for very low wind as well. As a result, the drag coefficient can be expected to exhibit a minimum at around $W_{10} \approx 5\ \text{m s}^{-1}$. These two reasons – the role of waves and the non-constancy of roughness – provide the most probable explanation for the overestimation of ε when (42.3) is applied naively, e.g. using nominal values for C_{10} from the literature (e.g. Lombardo and Gregg, 1989).

In the uppermost surface layers, the dissipation-rate profiles can deviate substantially from the LOW scaling due to the effect of surface wave breaking which contributes additional TKE (Fig. 42.2(b); see also Chapters 4 and 22 in this book). Kitaigorodskii and Lumley (1983), for instance, observed in Lake Ontario dissipation rates that were one to two orders of magnitude above those predicted by (42.3). The thickness of the wave-affected surface layer (WASL) scales with the wavelength λ_p, corresponding to the peak frequency of the surface waves f_p, and is about $^1/_2\lambda_p$. Hence this thickness is less in lakes than it is in the ocean and the unaffected LOW scaling beneath the WASL can be observed more frequently.

42.2.2 *Convective mixing*

Another source of TKE in the SBL is a positive, upward-directed surface buoyancy flux. This can be the result of surface cooling (thermal expansivity $\alpha > 0$), surface heating at temperatures below the temperature of maximum density (thermal expansivity $\alpha < 0$), or an increase in salinity due to evaporation. A unique feature of lakes is convection induced by penetrative radiation causing the water under ice to warm up.

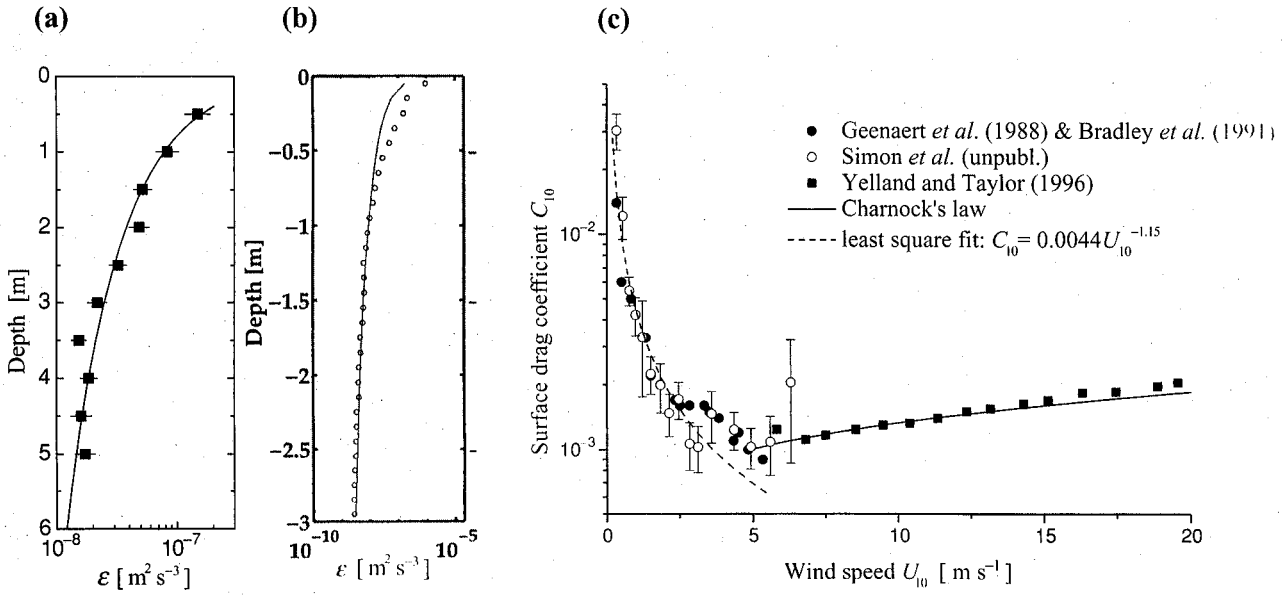

Fig. 42.2. (a) The profile of the dissipation rate ε measured in the Müggelsee (Germany). Measured dissipation rates (black boxes) with 95% confidence intervals and a fit to (42.3) are shown for an ensemble average of 31 individual microstructure profiles. (b) The same for a dissipation profile measured in Lake Neuchâtel (Switzerland), showing enhanced dissipation rates near the surface due to wave breaking. (c) The drag coefficient C_{10} determined using (42.3) from dissipation rates measured in a lake for various bins of wind speed (black dots) compared with oceanic values reported by Geernaert *et al.* (1988) and Bradley *et al.* (1991); open symbols indicate median values. The lines represent power-law fits to the data, as indicated by the equations. The error bars represent the 95% bootstrap confidence intervals. From Lorke and Wüest (2003). Copyright 2003 Annual Review.

In general, the production of TKE can be described by the surface buoyancy flux J_b, which can be quantified in the case of purely thermal forcing (disregarding the effect of increasing salinity due to evaporation) as follows:

$$J_b = -\frac{\alpha g}{c_p \rho} H_{net}. \tag{42.4}$$

In a recent study of nighttime convection in the absence of significant wind mixing by Jonas *et al.* (2003) convective plumes were tracked using a coherent acoustic Doppler current profiler (ADCP) (Fig. 42.3). Three cold nights during fall have been studied, featuring convective plumes (about 20 per night) reaching all the way down to the bottom of the mixed layer. The vertical component of the measured velocities allowed the identification of vertical convective plumes of horizontal width about 10 m. Surprisingly, it was observed that the convective layer is unstable only at the very top, leaving most of the convective layer stratified, and the plumes actually "tunnel" through the weakly stratified convective layer. Dissipation of TKE was almost homogeneous within the convecting "mixed-layer" zone but decreased by two to three orders of magnitude during the day (Jonas *et al.*, 2003).

In the case of convection due to surface cooling when the water temperature is above the temperature of maximum density (usually 4 °C), the source of energy is located at the very surface, and J_b in (42.4) equals the surface buoyancy flux J_b^0, whereas it is exponentially distributed throughout the depth where short-wave radiation is penetrating in the case of radiative heating when the temperature is below the temperature of maximum density. In the latter case, the total amount of TKE generation depends on the temperature gradient, $\partial T/\partial z$, and on the absorption coefficient of short-wave radiation A within the convective layer. The larger A the greater the amount of TKE produced, since warming becomes more restricted to the very-near-surface region where the buoyancy production is largest. The observation of radiatively driven convection under ice offers a unique opportunity to study "pure" convection without wind stirring. Figure 42.4 shows the development of the temperature under ice, measured in a Karelian lake by Malm *et al.* (1998).

42.3 The bottom boundary layer

The BBL is the second zone in lakes that is of great importance. However, here the main issue is not the exchange of energy or heat, but the fluxes of chemical elements and compounds across the boundary. Also, the

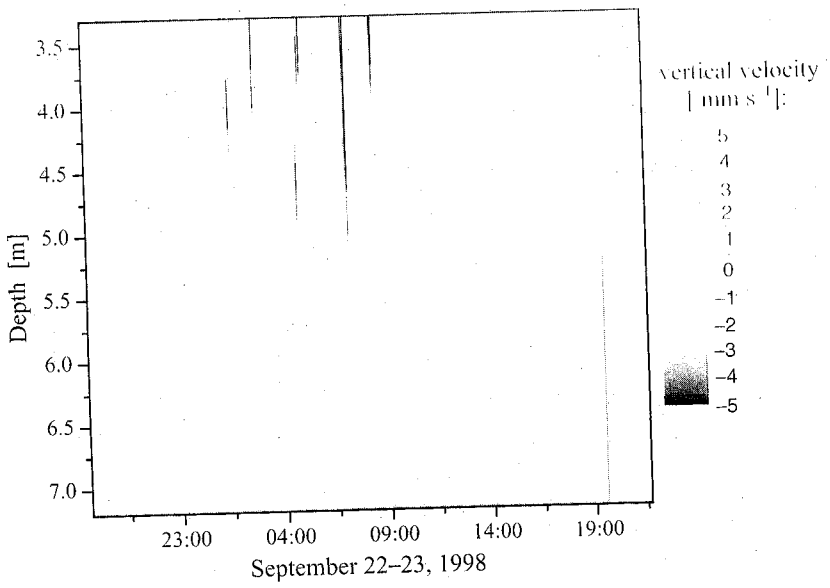

Fig. 42.3. Nighttime observations of convective plumes in the surface boundary layer of the Soppensee (Jonas *et al.*, 2003) obtained using the ADCP: red, upward; and blue, downward-moving thermals. The color-bar shows the scale of the vertical velocity in mm s^{-1}. In color on the CD.

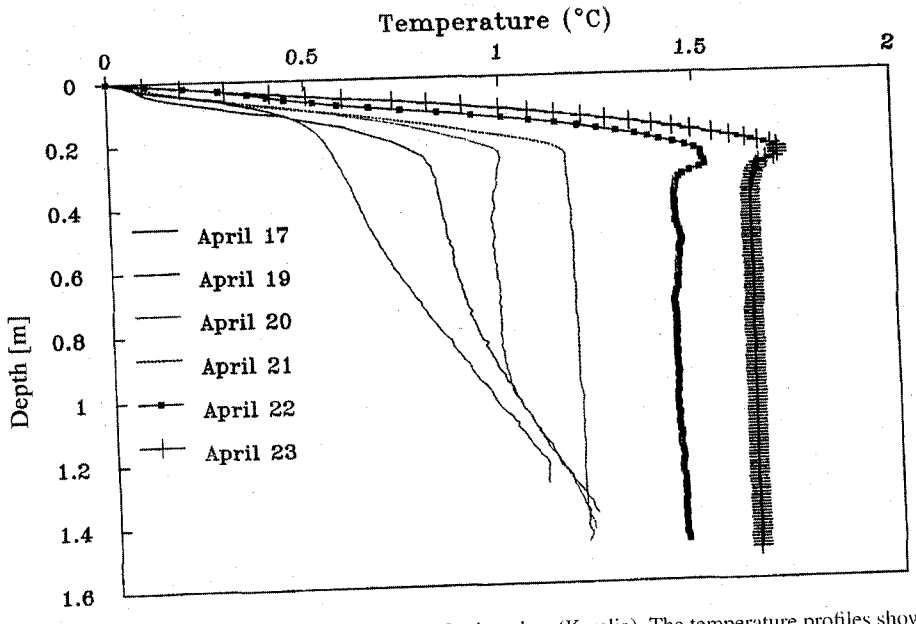

Fig. 42.4. The development of temperature beneath the ice in Lake Vendyurskoe (Karelia). The temperature profiles show the warming of the near-surface water by penetrating solar radiation. From Malm *et al.* (1998). Copyright 1998 ASLO.

sediment surface is rigid, and therefore the current velocity must fall to zero at the interface. Using this boundary condition and following the same argumentation as for the SBL, the LOW scaling leads to a logarithmic velocity profile $u(z)$, which can be described in terms of the bottom friction velocity u_f^b and the roughness length z_0:

$$u(z) = \frac{u_f^b}{\kappa} \ln(z/z_0). \tag{42.5}$$

The roughness length z_0 is related to sediment topography and can alternatively be expressed using a drag coefficient C_D, with

$$C_D = \frac{\kappa}{\ln(1\,\mathrm{m}/z_0)} \tag{42.6}$$

Depending on a length scale z_s that describes the bottom structure and the level of turbulence described by u_f^b, the flow regime is called *smooth* for $z_s \leq \nu/u_f^b$ and *rough*

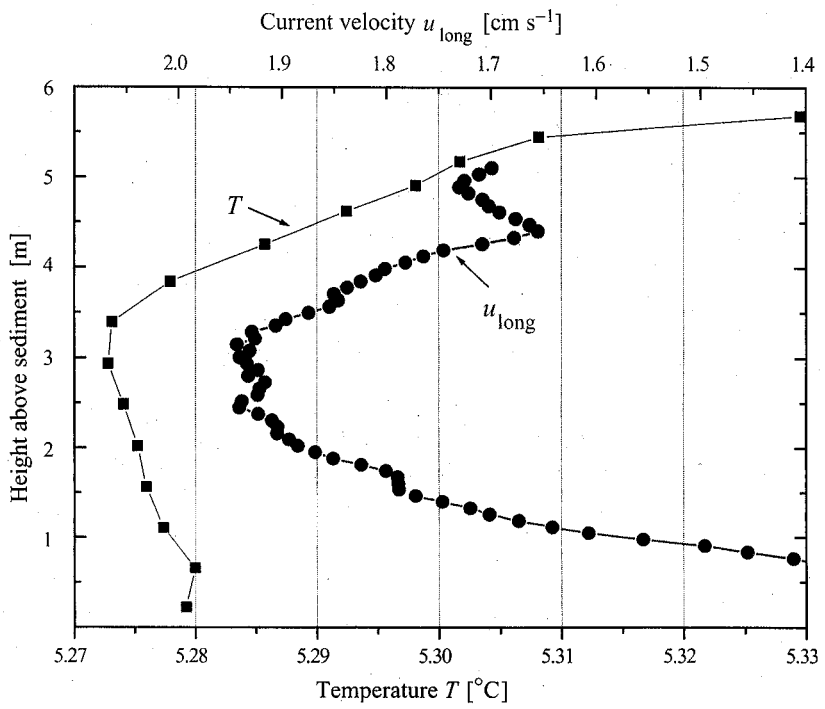

Fig. 42.5. The temperature T and longitudinal current velocity u_{long} measured in the BBL of Lake Alpnach under seiche-induced periodic forcing. The forcing with a period of 24 h produces a distinct velocity maximum between 2.5 and 3 m above the sediment. When the cold water, which was displaced horizontally by seiching, is flowing back, this velocity maximum produces unstable temperature stratification and hence strain-induced convection (Lorke *et al.*, 2002).

for $z_s \geq \nu/u_f^b$. For the smooth flow regime, the roughness length is $z_0 \approx 0.1\nu/u_f^b$ and hence does not depend on the sediment structure. For the rough flow regime, the roughness length can be estimated using $z_0 = z_s/30$.

It was found that not does only the small-scale sediment structure influence the velocity profile in the BBL, but also the sediment topography on larger scales (e.g. ripples) introduces an additional form drag.

Analogously to the case of the SBL, the dissipation rate of mechanical energy, ε scales inversely to the distance from the sediment, z, and is proportional to the cube of the friction velocity:

$$\varepsilon(z) = \frac{(u_f^b)^3}{\kappa z}. \tag{42.7}$$

By combining (42.5) with (42.7), the dissipation rate can be calculated from a fit of a measured logarithmic velocity profile to the LOW.

However, recent measurements in a lake have shown that dynamic effects like seiche-induced oscillatory currents affect the upper part of the velocity profile, and the validity of the LOW according to (42.5) and (42.7) is confined to within a few tens of centimeters above the sediment (Lorke *et al.*, 2002). Above this layer, the TKE budget cannot be regarded as a balance between production and dissipation and both the flux divergence and the rate term become of growing importance with increasing distance from the sediment. This differential divergence of TKE leads to a phase lag between the periodic forcing and dissipation. That means that the dissipation rate lags behind the current velocity by a delay within the range of minutes to hours, depending on the period of the seiching. In a low-energy system, this effect contributes significantly to the dynamics of turbulence in the BBL even for forcing periods as long as 24 h (Lorke *et al.*, 2002).

Another effect of the periodic forcing is a distinct velocity maximum that develops at a certain height above the sediment, and depends again on the period of the forcing and the level of turbulence. As shown in Fig. 42.5, this velocity maximum can produce instabilities in the stratification, resulting in the production of additional turbulence due to convection.[1]

In general, the enhanced energy dissipation due to bottom friction produces enhanced mixing in the BBL that maintains a well-mixed layer of height up to a few meters (Gloor *et al.*, 2000). However, resuspension of particulate matter as well as the density flux associated with

[1] Strain-induced convection analogous to the tidal straining in the ROFI regime described in Section 46.5 of this book.

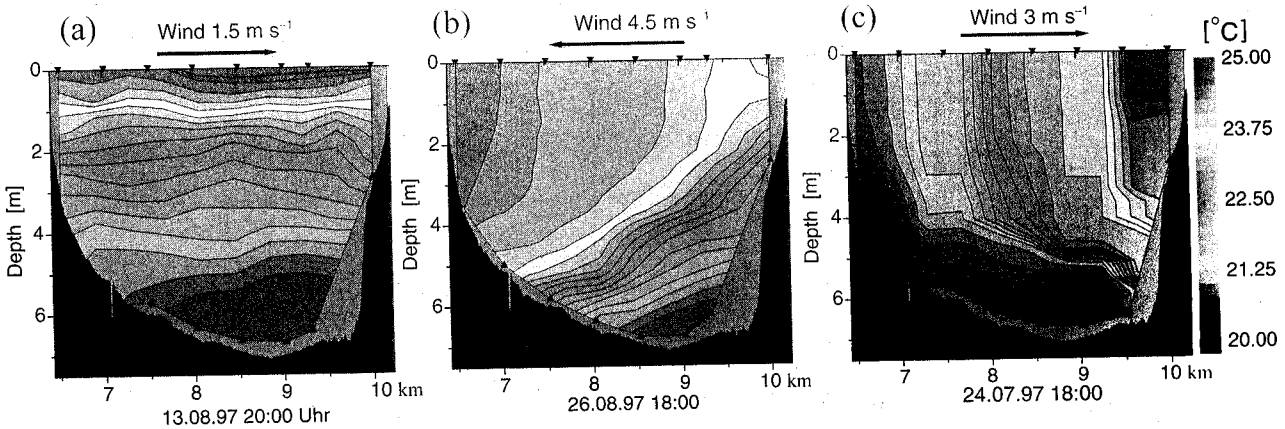

Fig. 42.6. Contour plots of termperature calculated from temperature–depth transects in the Müggelsee (Germany), showing the response of a shallow lake to various winds. The x axis characterizes a cross section through the near-elliptical lake. The prevailing wind directions and speeds are given above each plot. the Wedderburn numbers W were 7.0 in (a), 1.0 in (b), and 0.9 in (c). The mean stratification differed slightly between (b) and (c). Whereas in (b) the main temperature gradient occured in the lower part of the water column, in (c) stratification was stronger in the upper part. After the wind had ceased, the lake restratified horizontally and internal seiching became established in both cases. In color on the CD.

the redissolution of organic matter and calcite from the sediment tends to stabilize the BBL (the appearance of a chemocline). Because of the low current speed, resuspension is typically of less importance in lakes, and the diapycnal buoyancy flux in the deep water has been observed to vary strongly among lakes and can inhibit turbulent mixing completely (Wüest and Gloor, 1998).

42.4 Mixing in the interior

The main source of energy for turbulent mixing within the stratified interior of a lake is production of TKE by shear. Current shear is produced either by direct wind-driven circulation (which is more important in the upper pycnocline) or by internal waves or seiches.

Wind stress acting on the surface of a lake can produce upwelling of metalimnetic or even hypolimnetic water at the upwind end of the lake, as illustrated in Fig. 42.6. The response of the lake can be described by two non-dimensional numbers, the Wedderburn number, W, and the lake number, L_N (Imberger, 1998).

The Wedderburn number describes the balance between the surface wind stress and the baroclinic pressure gradient resulting from the slope of the interface in a two-layer system with a density difference ρ' in a rectangular basin,

$$W = \frac{g' h_1^2}{u_f^2 L}, \tag{42.8}$$

where h_1 is the thickness of the upper layer, g' is the reduced gravitational acceleration across the interface, $g' = g\rho'/\rho$, and L is the characteristic length of the basin. When W decreases, the interface tilts more and more until it surfaces at the upwind end of the lake when W is about unity. This process is illustrated in Fig. 42.6. However, Figs. 42.6(b) and (c) also show that the response of the lake for comparable Wedderburn numbers (both are around unity) can be quite different, depending on the detailed structure of stratification.

The lake number L_N is defined similarly to W but accounts for a more realistic density distribution in terms of stratification and topography (Imberger and Patterson, 1990). Whereas W is a suitable number to describe upwelling of metalimnetic water with h_1 taken as the depth of the diurnal thermocline, L_N can describe potential upwelling of hypolimnetic water if the seasonal thermocline reaches the surface.

If, due to the mechanism described above, a deep thermocline reaches the surface and the wind continues blowing, the isotherms in the epilimnion become vertical and a completely two-dimensional mixing mechanism can occur. This phenomenon, which was described by Monismith (1986) on the basis of laboratory experiments, occurs in the situation given by Fig. 42.6(c). That is, this phenomenon may be important in shallow lakes.

42.4.1 Seiching

Another effect of wind, which exerts a stress on the water surface, is the excitation of seiches. Seiches are basin-scale standing surface (barotropic) or internal (baroclinic) waves and are a unique and prominent feature in lakes and other enclosed water bodies such as bays and fjords. The time series and velocity spectra of current components in Fig. 42.7 illustrate three possible first-mode oscillations in a medium-sized lake in Switzerland. The first possible

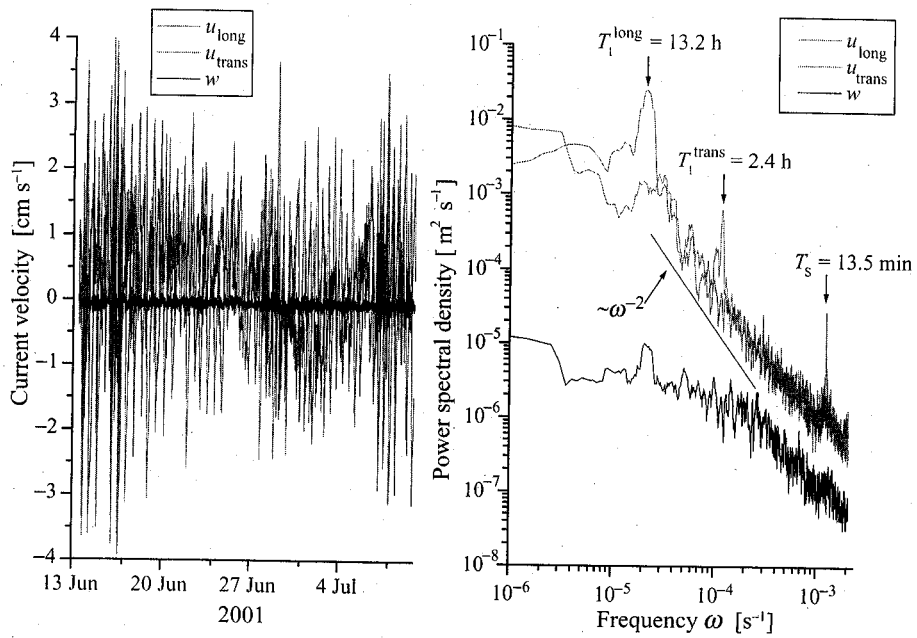

Fig. 42.7. Time series (left-hand panel) and spectra (right-hand panel) of the three velocity components along the main lake axis (u_{long}), normal to the lake axis (u_{trans}), and vertical (w). The measurements were carried out in the BBL of Lake Hallwil (Switzerland), revealing intense internal seiching along the two axes of the lake and external (surface) seiching along the main axis (data by courtesy of D. McGinnis, unpublished). The periods of the local spectral maxima correspond well to the classical estimates (42.9) and (42.10). The line $\sim \omega^{-2}$ in the spectrum plot shows the universal slope of high-frequency internal waves (Garret and Munk, 1972). In color on the CD.

response of a lake to a wind-event forcing is barotropic, surface, or external seiching, whereby the whole water body is oscillating, leading to almost periodic displacements of the lake surface.

The periods T_S of these oscillations are related to the horizontal scale of the lake, L, and to the typical depth H of an equivalent rectangular basin through

$$T_S = \frac{2L}{\sqrt{gH}}. \tag{42.9}$$

T_S ranges typically from minutes (for small-to-medium-sized lakes) to a few hours (for the largest lakes on Earth). Surface displacement amplitudes and associated current velocities are small and thus the impact on the production of TKE (shear production) is rather small. Nevertheless, even small-amplitude seiches may cause harmful floods over large areas when the environment of the lake is flat. This is the case for some shallow embayments of the Baltic Sea, for instance.

Internal or baroclinic seiching leads typically to much higher displacement amplitudes, for instance in Lake Constance up to several meters and even tens of meters, depending on the forcing. It is based on displacements of internal interfaces, e.g. the thermocline. The application of a simple two-layer approximation in a rectangular basin leads to the Merian formula, giving the eigenperiod of the ith mode T_i as a function of the two layer thicknesses h_1 and h_2 and of the reduced gravitational acceleration g'. A first-mode response ($i = 1$) can be observed in many lakes with periods between hours (for small-to-medium-sized lakes) and weeks (for large lakes) with thermocline displacements of up to several tens of meters.

$$T_i = \frac{1}{i}\frac{2L}{\sqrt{g'h_1h_2/H}}. \tag{42.10}$$

The eigenmodes described by (42.10) are so-called horizontal modes. By adding more layers to the model in order to describe a more realistic density profile, a second "quantum number" j can be introduced, describing vertical modes of oscillation.

42.4.2 The effect of the Earth's rotation

In large lakes, the effects of the Earth's rotation are no longer negligible and internal Kelvin, Poincaré or topographic waves as well as inertial waves develop, resulting in a three-dimensional structure of isotherm displacements. (For recent observations and model results see e.g. Hutter *et al.* (1998), Saggio and Imberger (1998), Antenucci *et al.* (2000), and Hodges *et al.* (2000)).

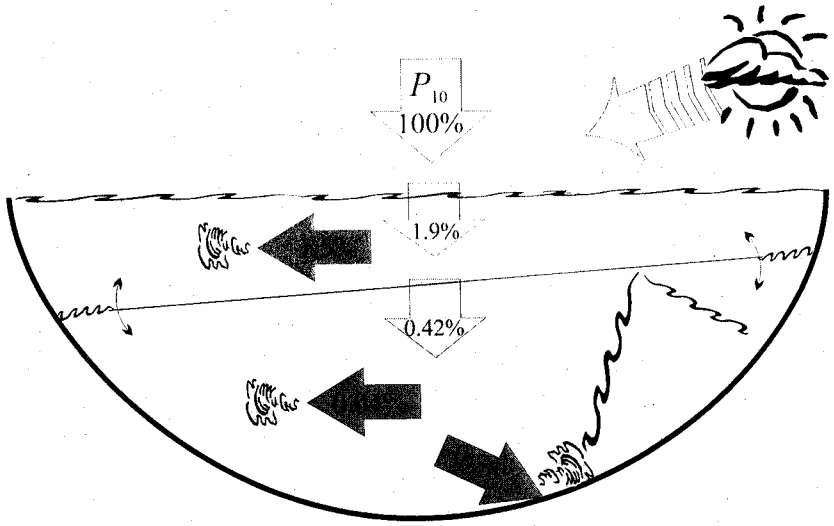

Fig. 42.8. The flux of turbulence energy estimated in Lake Alpnach (Switzerland) during dominant wind forcing following Wüest *et al.* (2000a): 1.9 % of the estimated vertical wind energy flux P_{10} (measured 10 m) above the lake's surface was available for wind mixing in the entire lake; 1.5% of P_{10} was dissipated by turbulence in the surface mixing layer and contributed to mixing processes in this region. The remaining 0.4% was transferred to the stratified hypolimnion by internal seiching. Of this portion, 90% was dissipated in the BBL and only 10% was available for mixing the interior of the lake.

42.4.3 High-frequency internal waves

The thermocline as well as the stratified hypolimnion of lakes also supports smaller-scale internal waves with frequencies between the inertial and the buoyancy frequency N. The internal-wave spectrum within this frequency range follows the same ω^2 shape as that described by Garret and Munk (1972) for the ocean and by Imberger (1998), MacIntyre *et al.* (1999), Stevens (1999), and Thorpe (1998) for lakes (see also Fig. 42.7).

Generally it is assumed that the internal waves dissipate their energy in the interior by wave breaking. However, direct measurements of turbulence and mixing in the interior of stratified lakes using the microstructure technique have shown that turbulent mixing is rather weak (e.g. Wüest *et al.* 2000a; Etemad-shahidi and Imberger, 2001). Analogously to the case of the ocean, it was found that local diffusivities estimated from microstructure measurements are on average one order of magnitude less than diffusivities inferred indirectly from tracer observations by integrating over much larger horizontal scales (Gregg, 1987b; Wüest and Gloor, 1996).

As discussed in Chapter 16 of this book, two different tracer experiments conducted in a medium-sized lake revealed the importance of boundary mixing for the basin-wide diapycnal matter fluxes (Wüest and Gloor, 1996; Goudsmit *et al.*, 1997). The latter investigation showed clearly that the vertical spreading of a patch of tracer injected into the hypolimnion of the lake increased by approximately one order of magnitude as soon as the tracer cloud reached the lake boundary. Comparable results were obtained from similar tracer studies in the ocean by Ledwell and Bratkovich (1995) and by microstructure investigations in a lake by MacIntyre *et al.* (1999).

42.5 Summary

By combining the three distinct zones discussed above, the flux path of mechanical energy in a lake (Imberger, 1998) can be redrawn. Wüest *et al.* (2000a) estimated the relative importance of the different sources of vertical mixing in a simply shaped lake basin as illustrated in Fig. 42.8 by compiling data from various studies on lakes. Wind introduces mechanical energy into the lake in two fundamentally different ways. First, most of the energy is introduced directly into the surface layer (a) by driving the basin-wide circulation accompanied by creating shear stress in the surface layer (see LOW in Fig. 42.2) and (b) by surface-wave acceleration and subsequent wave breaking (see WASL in Fig. 42.2). This TKE is available for turbulent mixing in the SBL and also for entrainment if the amount of energy is sufficient for thermocline erosion.

A second flux path is the introduction of kinetic energy by setting up internal waves or basin-scale modes. Only a small portion of this energy is dissipated in the interior due to internal shear production and most of the energy is transferred to the BBL via high-frequency internal waves

breaking at the sloping bottom (e.g. Thorpe, 1998) and by bottom friction (see BBL in Section 42.3).

The basin-wide mixing efficiency for an entire stratified water body (hypolimnion) was estimated to be $\Gamma \approx 0.15$ for the extensively studied Lake Alpnach (see Fig. 42.8). This mixing efficiency, representative of a large-scale volume, is in surprisingly good agreement with independent microstructure-based estimates of Γ (e.g. Osborn, 1980; Oakey, 1982). Comparison with TKE balances performed for other lakes (Wüest *et al.*, 2000a) demonstrates that this analysis is representative for many of them, as long as wind is the dominant source of TKE.